

## Important kinetic effects in the hybrid ElectricOIL system

Joseph W. Zimmerman<sup>a,b</sup>, Darren M. King<sup>a</sup>, Andrew D. Palla<sup>a</sup>, Joseph T. Verdeyen<sup>a</sup>,  
David L. Carroll<sup>a</sup>, Julia K. Laystrom<sup>a</sup>, Gabriel Benavides<sup>a</sup>, Brian S. Woodard<sup>b</sup>,  
Wayne C. Solomon<sup>b</sup>, W. Terry Rawlins<sup>c</sup>, Steve J. Davis<sup>c</sup>, Michael C. Heaven<sup>d</sup>

<sup>a</sup>CU Aerospace, Urbana, IL 61820

<sup>b</sup>University of Illinois at Urbana-Champaign, Urbana, IL 61820

<sup>c</sup>Physical Sciences Inc., Andover, MA 01810

<sup>d</sup>Emory University, Atlanta, GA 30322

### ABSTRACT

Laser action at 1315 nm on the  $I(^2P_{1/2}) \rightarrow I(^2P_{3/2})$  transition of atomic iodine has been obtained by a near resonant energy transfer from  $O_2(a^1\Delta)$  produced using a low-pressure electric discharge. In the electric discharge oxygen-iodine laser (ElectricOIL) the discharge production of atomic oxygen, ozone, and other excited species adds significantly higher levels of complexity to the post-discharge kinetics which are not encountered in a classic purely chemical  $O_2(a^1\Delta)$  generation system. In this paper, the discharge species output for laser operating conditions are discussed. Spatial measurements of  $O_2(a^1\Delta)$  and  $O_2(b^1\Sigma)$  are reported, and various methods for the determination of atomic oxygen levels are discussed and compared. The injection of  $NO_x$  into the system to benefit  $O_2(a^1\Delta)$  production is investigated.

**Keywords:** oxygen-iodine laser, ElectricOIL, DOIL, post-discharge oxygen kinetics, singlet-delta oxygen, titration, actinometry

### 1. INTRODUCTION

The classical chemical oxygen-iodine laser first reported by McDermott<sup>1</sup> operates on the electronic transition of the iodine atom at 1315 nm,  $I(^2P_{1/2}) > I(^2P_{3/2})$  [denoted hereafter as  $I^*$  and  $I$  respectively]. The lasing state  $I^*$  is produced by near resonant energy transfer with the singlet oxygen metastable  $O_2(a^1\Delta)$  [denoted hereafter as  $O_2(a)$ ]. Conventionally, a chemical two-phase process is used to produce the  $O_2(a)$  at the interface of liquid basic  $H_2O_2$  and  $Cl_2$  gas. In efforts to produce a more efficient system, Zalesskii<sup>2</sup> and Fournier<sup>3</sup> made early attempts to use electric discharges for  $O_2(a)$  production and transfer energy to iodine for lasing, but were unable to obtain positive gain. Since then, various groups<sup>4-9</sup> have investigated similar continuous flowing systems and have measured  $O_2(a)$  yields in excess of 15%, a necessary condition for positive gain at room temperature. However, it was not until the work of Carroll et. al.<sup>10</sup> that positive gain was achieved, with lasing in the same system reported in subsequent work<sup>11</sup>. The key difference between the traditional chemical excitation route and the electrical one is the presence of copious amounts of atomic oxygen. Atomic oxygen depletes the upper laser level and must be controlled<sup>12,13</sup>. This was accomplished by the use of  $NO_2$  in a titration made downstream from the discharge or by adding  $NO$  to the discharge flow or downstream of the discharge.

In this work, the kinetic effects observed in the system reported by Carroll et. al.<sup>10-12</sup> are explored, with a focus on the interaction of  $NO_x$  sensitizers on the production and levels of  $O_2(a)$  and atomic oxygen. First, the experimental setup and diagnostics will be discussed. Second, the various techniques applied for measuring oxygen atoms in the flow system will be reviewed, noting difficulties. These techniques are (i)  $NO_2$  titration method, (ii)  $NO$  titration / PMT calibration method, and (iii) the trace argon-oxygen actinometry method. Third, the spatial behaviors of important species will be reported, and fourth, the catalytic effects of  $NO$  on  $O_2(a)$  production will be discussed.

### 2. EXPERIMENTAL APPARATUS

A block diagram of the typical flow tube setup for laser operation is shown in Figure 1. The supersonic diagnostic cavity has a Mach 2 nozzle with windows mounted along the divergent section that serve as view ports, and can be reconfigured to support 1" mirror mounts. Upstream of the nozzle, the subsonic diagnostic duct has four windows through which simultaneous measurements are made of the optical emission from  $O_2(a)$  at 1268 nm,  $O_2(b^1\Sigma)$  [denoted

O<sub>2</sub>(b) hereafter] at 762 nm, I\* at 1315 nm, and the gain/absorption proportional to [I\*] – 0.5·[I]. Optical emission data are also taken directly through glass tubes in the flow system, which can be reconfigured for a variety of studies. A Roper Scientific Optical Multi-channel Analyzer (OMA-V) was used for measurements at 1268 nm. An Apogee E47 CCD camera coupled to a Roper Scientific/Acton Research 150-mm monochromator was implemented to measure the emission of O<sub>2</sub>(b) at 762 nm, as well as the emissions of excited atomic oxygen at 777 nm, and excited argon at 750.4 nm. The broadband emission of NO<sub>2</sub>\* was measured using a Hamamatsu R955 photomultiplier with a narrowband 580 nm filter and a 50 mm focal length Pyrex collection lens. All optical diagnostics were fiber coupled using Oriel model #77538 glass fiber bundles.

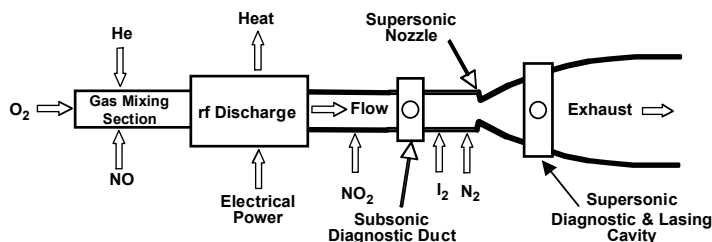


Figure 1: Schematic of typical ElectricOIL experimental apparatus.

Micro-Motion CMF and Omega FMA mass flow meters were used to measure the flow rates of the gases. Pressures in the flow tubes were measured by capacitance manometers. Incident and reflected powers to the radio-frequency (RF) matching network were measured by a Bird ThruLine model 43 wattmeter (RF “System Power” is the difference of the incident and reflected powers). A longitudinal discharge with two hollow cathodes inside a 5 cm diameter quartz tube was used with a standard electrode separation of 25.4 cm. The discharge was excited with (RF) power at 13.56 MHz. For the kinetics studies here, various flow tube and injector configurations were used and are discussed as necessary.

### 3. METHODS FOR MEASURING OXYGEN ATOM YIELDS

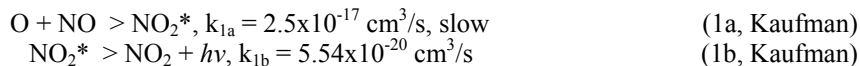
From previous work, atomic oxygen is known to play a vital role in the hybrid electric oxygen-iodine laser system. The dominating factor is the power efficiency lost in quenching of I\* by O-atoms. Secondly, atomic oxygen plays a role in dissociating injected I<sub>2</sub>. These effects were described by Carroll et. al.<sup>12</sup> and modeled by Palla et. al.<sup>13</sup>. The key result is that NO<sub>2</sub> injected downstream could be used to control the atomic oxygen level as necessary: high enough to dissociate I<sub>2</sub> rapidly, and low enough such that the influence of the I\*+O loss is marginal. Without NO<sub>2</sub> in the flow, the addition of ~0.006 mmol/s of I<sub>2</sub> to 16:4 mmol/s He:O<sub>2</sub> at 10 Torr resulted in nearly 80% loss of peak O<sub>2</sub>(a) signal (with 500 W RF power).<sup>12</sup> Titrating with NO<sub>2</sub> downstream of the discharge and upstream of the I<sub>2</sub> injection led to progressively increased O<sub>2</sub>(a) signal, with the level returning to that of the zero I<sub>2</sub> case with 1 mmol/s of NO<sub>2</sub> injected. The 1315 nm (I\*) and 762 nm (O<sub>2</sub>(b)) emissions benefited similarly.

In concurrent work by this group<sup>12</sup>, O<sub>2</sub>(a) production in the discharge was enhanced by adding trace amounts of NO to the discharge flow. Originally, this benefit was attributed to lowered gas ionization potential, leading to a discharge with an E/N (electric field to gas density ratio) more optimal for O<sub>2</sub>(a) production. However, in recent work discussed herein, this effect is likely a combination of the effect of NO on the discharge, and its effect on atom recombination in the discharge and post discharge regions through a significant branching fraction to O<sub>2</sub>(a) from the O+NO<sub>2</sub> reaction.

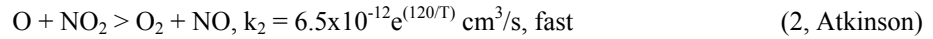
Thus, the level of atomic oxygen in the system must be known and controlled in order to maintain high yields and develop favorable conditions for lasing. In order to gain knowledge of atomic yields in the ElectricOIL system, various methods for deducing [O] have been applied.

#### 3.1 Air afterglow method 1: Kaufman titration technique

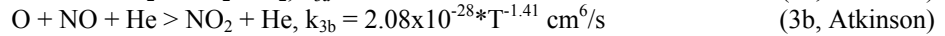
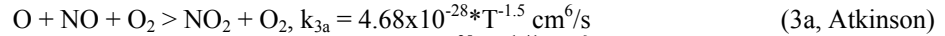
One atomic oxygen measurement technique applied is the NO<sub>2</sub> titration method as presented by Kaufman<sup>14</sup>. In this technique, a photo-multiplier tube (PMT) is used to measure the air afterglow emission from the reactions (1a) and (1b),



as NO<sub>2</sub> is added to the flow. The NO for this reaction is rapidly produced by the fast harpoon reaction



which is highly exothermic (1.995 eV) and may result in O<sub>2</sub>(X), O<sub>2</sub>(a), or O<sub>2</sub>(b). The atoms are depleted by reaction (2) and by three-body recombination. Reactions (3a) and (3b) respectively are published rates for air (applied to oxygen) and argon (applied to helium).



As NO<sub>2</sub> is added, the emission from reaction (1) increases with NO formed by reaction (2); the emission then reaches a peak, and then begins to decrease as atoms are depleted by reaction (2). Kaufman found that the NO<sub>2</sub> flow rate corresponding to the peak emission corresponds to half the flow rate required to extinguish the emission, and therefore fully titrate atoms. Thus, the peak in the fluorescence as a function of NO<sub>2</sub> flow rate can be used to determine the level of atoms for various discharge flows and power settings.

Problems with this technique are that the peak in fluorescence is not independent of distance from the plane of titration and is affected by mixing of the NO<sub>2</sub> into the discharge effluent, especially in the fast flowing high pressure devices used in these studies. In other words, there are two regions in the flow between the injector and observation point: (i) the mixing region, near the injector, where NO<sub>2</sub> is converted to NO, and oxygen atoms rapidly depleted by reaction (2), and (ii) the three-body decay region, where NO<sub>2</sub> has been almost completely converted to NO, and the observed oxygen atom density is subject to decay from a two-step process of reaction (3) followed by reaction (2). This suggests that the observed intensity  $I_{\text{obs}}$  be corrected by some decay factor such that  $I_{\text{obs}} = I_{\text{cor}} \cdot \exp(-\alpha t)$ , where  $I_{\text{cor}}$  is the corrected intensity, and  $\alpha$  is the decay rate representing the losses from three-body and wall recombination. Past data taken by our group suggested that the peak in the intensity versus NO<sub>2</sub> flow rate curve is fairly constant with distance, making the correction unnecessary. However, this correction will likely be implemented as pressure and diluent flow rates increase, enhancing recombination effects.

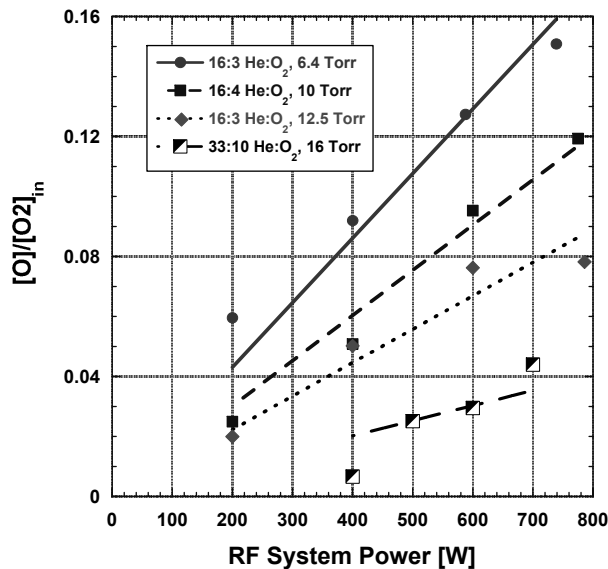


Figure 2. Oxygen atom yields versus RF system power for typical flow rates.  $[\text{O}]/[\text{O}_2]_{\text{input}}$  is taken to be the flow rate determined from the NO<sub>2</sub> titration method divided by the input flow rate of oxygen. Fits are linear through zero.

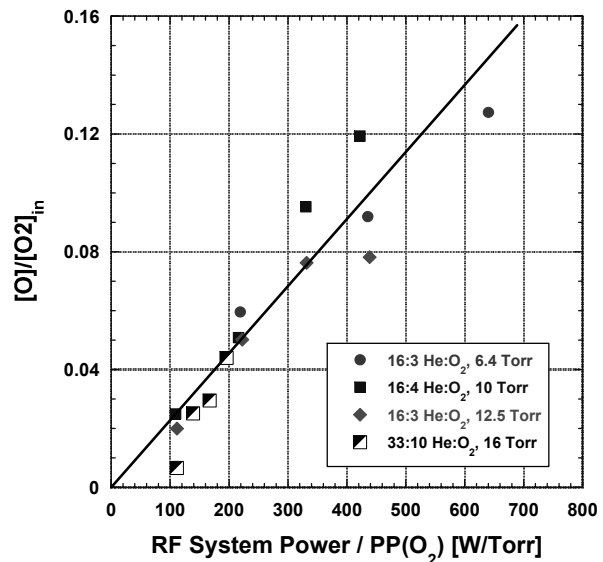


Figure 3. Oxygen atom yields versus power per O<sub>2</sub> partial pressure for typical flow rates.  $[\text{O}]/[\text{O}_2]_{\text{input}}$  is taken to be the flow rate determined from the NO<sub>2</sub> titration method divided by the input flow rate of oxygen.

Figure 2 shows oxygen atom yields for various flow rates when the Kaufman titration method is applied to He:O<sub>2</sub> discharges. For the 16:3 mmol/s He:O<sub>2</sub> case, halving the pressure results in a doubling of the slope of oxygen atom yield with power. The 33:10 He:O<sub>2</sub> case at 16 Torr, typical of laser operation flow rates, results in significantly lower oxygen atom yield. Figure 3 shows the atomic oxygen yields from Fig. 2 as a function of the ratio of system power to O<sub>2</sub> partial pressure, PP(O<sub>2</sub>). The data approximately follow a linear increase as a function of specific power as predicted by Stafford<sup>15</sup>.

The Kaufman NO<sub>2</sub> titration technique using the peak of the NO<sub>2</sub>\* emission has yielded consistent and repeatable results for He:O<sub>2</sub> discharges, but has the puzzling characteristic that the peak of the fluorescence does not appear at half the flow rate for extinction of the air-glow as originally stated. We have attributed this behavior to non-uniform mixing of the NO<sub>2</sub> into the discharge effluent, and the fast flow conditions of our system.

### 3.2 Air afterglow method 2: PMT calibration using N<sub>2</sub> discharge

The second O-atom measuring technique which has been applied in our lab is described by Piper<sup>16</sup>. In this technique, the effluent of a N<sub>2</sub>/Ar discharge and NO titration are used to calibrate the PMT to the signal produced by reaction (1). The technique follows this procedure: (1) the power on the discharge is held constant, producing a “constant” flow of nitrogen atoms; (2) at some downstream location, NO is injected incrementally; (3) a filtered PMT downstream of NO injection measures the afterglow emission produced by excited nitrogen formed by 3-body recombination,



and the air afterglow emission from reaction (1) (green glow). The titration of nitrogen atoms occurs by the fast reaction



which also produces oxygen atoms to create the air afterglow from reaction (1). The kinetics of the titration are described in Table 1. With increasing NO flow rate, the point at which the yellow glow is extinguished gives the concentration of nitrogen atoms produced by the discharge. From that point on, the oxygen atom concentration produced by reaction (5) is invariant with NO, and a calibration factor for the PMT can be determined by Eqn. (6).

$$K = \frac{1}{[O]_0} \frac{dI}{d[NO]} \quad (6)$$

Here, [O]<sub>0</sub> is the concentration determined from the nitrogen titration endpoint, and dI/d[NO] is determined from the slope of green airglow with increased NO flow beyond the endpoint. Applied to oxygen discharge effluent, the atomic oxygen flow rate is found with the calibrated PMT by [O] = I/(K\*[NO]).

Table 1: A description of air afterglow method 2.

State	Condition	Description	Behavior
[N] >> [NO]	NO is limiting reagent	[O] is identical to injected [NO], yellow glow created by reaction 4	Yellow glow linearly proportional to [N] <sup>2</sup>
[N] = [NO]	N-atom titration endpoint	Endpoint determines [N] produced by discharge	Yellow glow extinguished
[N] << [NO]	N is limiting reagent	[N] completely converted to [O], [O] is invariant with [NO], green afterglow created by reaction 1	Green glow linearly proportional to [NO]

Figure 4 shows the PMT data for NO titration downstream of a 40 W microwave discharge in a mixture of 8.8 % N<sub>2</sub> in Ar at 8.4 Torr. The air afterglow is corrected for three-body and wall recombination (assuming constant temperature) using

$$I_{\text{cor}} = I_{\text{obs}} e^{\alpha t}, \quad \text{where } \alpha = 2 \sum_M k_M [NO][M] + k_{\text{wall}} \quad (7)$$

where  $t$  is the flow time between injection and the observation points,  $I_{\text{cor}}$  is the corrected intensity,  $I_{\text{obs}}$  is the observed intensity,  $k_{\text{wall}}$  is the wall recombination rate, and the first term in  $\alpha$  is the sum of three-body rates, with the factor of 2 coming from the assumed fast reaction with  $\text{NO}_2$  which is formed by the three-body processes.

Using this corrected calibration factor for the PMT determined from Fig. 4, the results from the  $\text{NO}_2$  titration technique and the calibrated  $\text{NO}$  titration technique were compared, as shown in Fig. 5. The data shown for both methods are corrected for three-body effects. The two methods result in similar atom flow rates, with the  $\text{NO}$  titration method displaying a non-linear trend with power. The deviation at higher powers appears to be due to uncertainty in the temperature dependence of the air afterglow intensity, which requires further investigation. Figure 6 shows the data used to apply the calibrated PMT method; these data exhibit a non-linear trend with  $\text{NO}$  flow rate, which can be corrected for recombination effects.

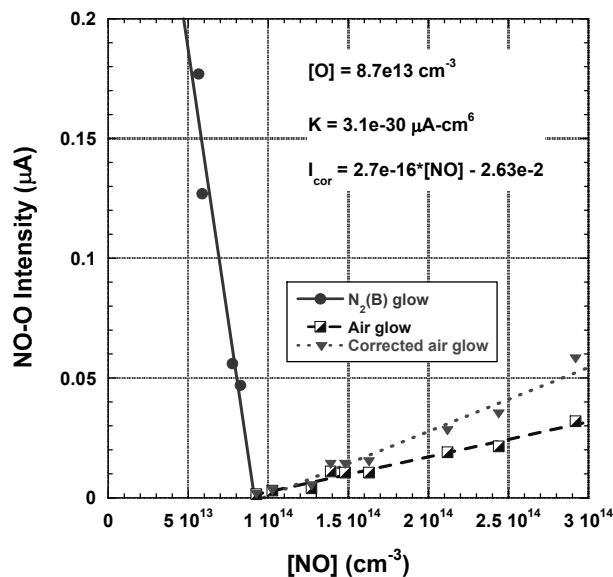


Figure 4. PMT signals for air afterglow titration using microwave discharge in  $\text{Ar}:\text{N}_2$  mixture. The flow is 8.8%  $\text{N}_2$  in  $\text{Ar}$  diluent at 8.4 Torr, and the microwave power level is 40 W.

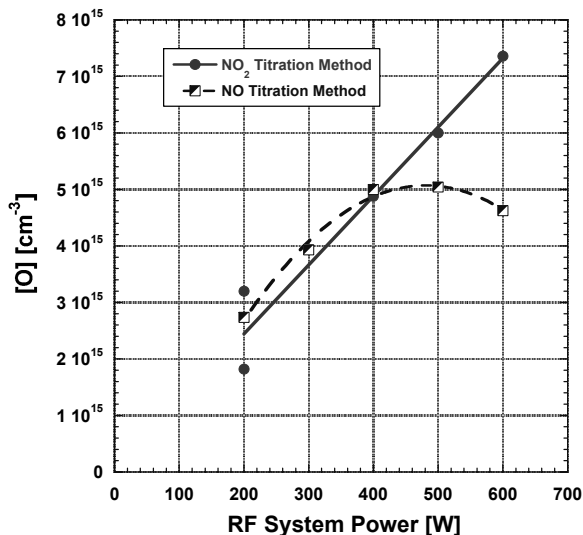


Figure 5. A comparison of afterglow methods for determining oxygen atoms. Flow conditions are 16:4 mmol/s  $\text{He}:\text{O}_2$  at 10 Torr. The calibrated PMT method uses  $\text{NO}$  varying from 0.1 to 0.5 mmol/s.

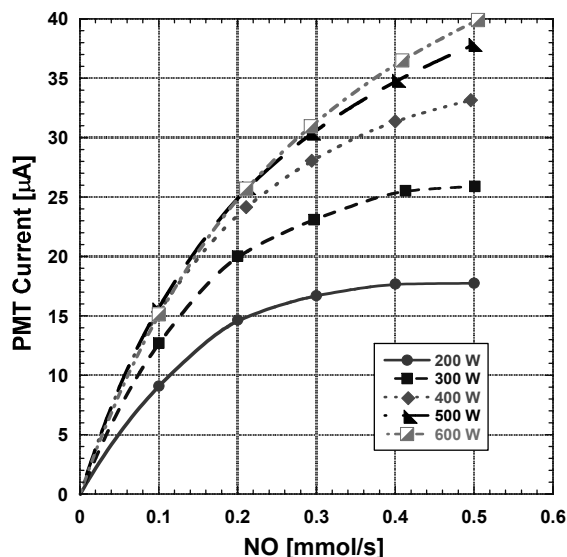


Figure 6.  $\text{NO}_2^*$  emission vs.  $\text{NO}$  flow rate for varied RF power. The discharge flow is 16:4  $\text{He}:\text{O}_2$  at 10 Torr. The PMT is 20 cm downstream of titration injection.

### 3.3 Complications of applying air afterglow methods in the ElectricOIL system

The most serious difficulty met when measuring O-atoms in the ElectricOIL system is that both titration methods fail to yield simple interpretation when NO is added to the discharge. When NO<sub>2</sub> or NO is added downstream of the discharge to a flow already containing trace NO, the air-glow fluorescence decreases, suggesting that the NO in the discharge effluent has already decreased the atomic oxygen to less than the NO flow rate. Hence, any new NO created by reaction (2) reduces [O] further, leading to decreased fluorescence from reaction (1). Further work is needed to understand this effect, but it is clear that either air-glow titration method is complicated by the presence of NO in the discharge.

Figure 7 shows the effect of NO<sub>x</sub> titration on another typical discharge flow of 33:10 mmol/s He:O<sub>2</sub> at 16 Torr with 500 W RF power (no NO present in discharge effluent). In this case, only five times the amount of NO is required to maximize and rollover the NO<sub>2</sub>\* signal as compared to the NO<sub>2</sub> titration. With typical use of 0.15 mmol/s of NO through the discharge in an operational laser case, the oxygen atom decay is significantly influenced. Figure 8 shows the effect of NO flowing through the discharge on the titration of oxygen atoms with NO<sub>2</sub>. The change in the fluorescence with increasing NO<sub>2</sub> is negative in the presence of NO effluent, negating the use of the NO<sub>2</sub> titration method. However, the flow rate required to extinguish the emission at the measurement plane in the case with 0.15 mmol/s NO is about a third that of the zero NO case, suggesting a significantly lower atom flow rate. The effect is similar when the second afterglow technique using NO is applied. Although the second method uses a calibration of the PMT which should allow for negative slopes, determining proper corrections is difficult, and should be the subject of further investigation (see Figs. 6 and 7).

Figure 9 shows the decay of the NO<sub>2</sub>\* emission for varied power and pressure, flowing 16:3:0.15 mmol/s He:O<sub>2</sub>:NO through the discharge. The signal decay is exponential, faster with higher pressure as expected, representing significant spatial decay of atoms with NO present. Figure 10 plots a modeling result for the effect of reaction (3b) on the decay of oxygen atoms with a titration flow rate of 0.2 mmol/s NO<sub>2</sub>. The addition of the three-body mechanism leads to significantly faster decay, because it serves both to recombine atoms and more importantly, to recycle NO<sub>2</sub>, fueling the fast decaying effect of reaction (2). The data described here suggest that the use of air afterglow methods to determine oxygen atom flow rates becomes a difficult task when NO is used as a sensitizer. Therefore, less invasive methods which are unaffected by the effluent kinetics must be applied.

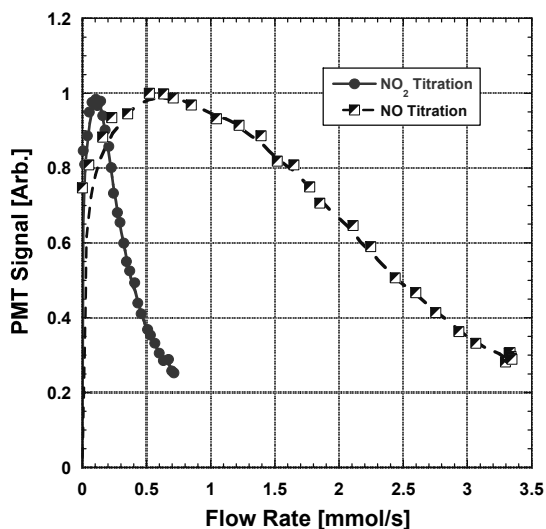


Figure 7. NO<sub>2</sub>\* signal vs. titration flow rate. The discharge flow is 33:10 He:O<sub>2</sub> at 16 Torr. The discharge power is 500 W RF. The PMT is 20 cm downstream of titration injection.

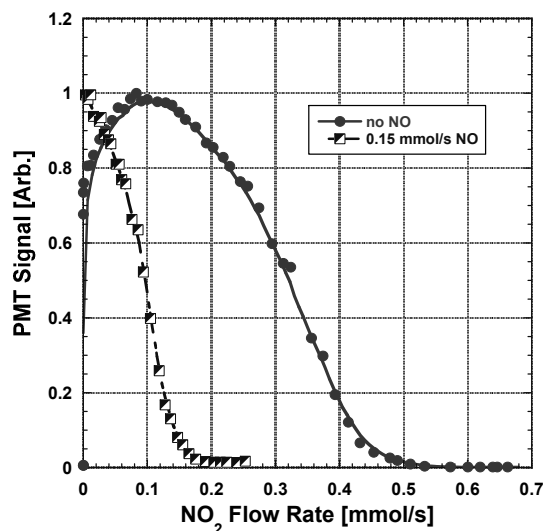


Figure 8. NO<sub>2</sub>\* signal as a function of NO<sub>2</sub> flow rate with and without NO in the discharge flow. The discharge flow is 16:3 He:O<sub>2</sub> at 12.5 Torr, with 500 W RF.

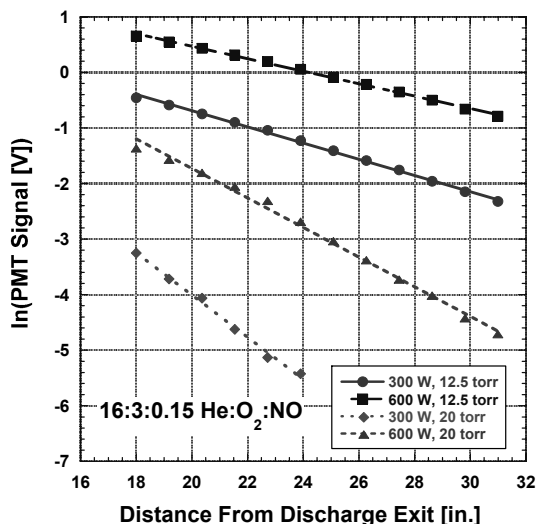


Figure 9. Log of  $\text{NO}_2^*$  signal as a function of distance from the discharge exit for varied pressure and RF power. The discharge flow is 16:3:0.15 He: $\text{O}_2$ :NO.

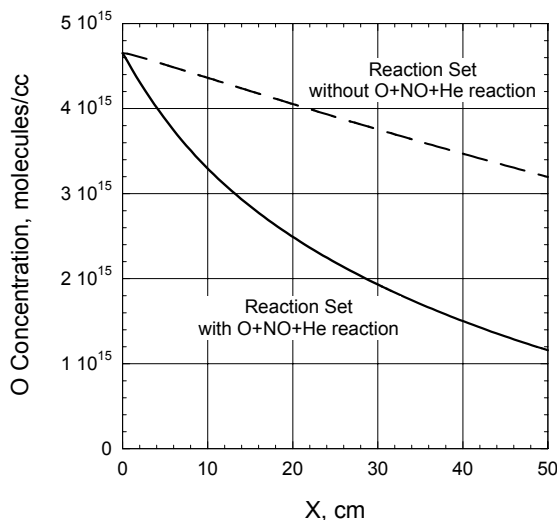


Figure 10. Oxygen atom decay from Blaze-II modeling result (Palla<sup>13</sup>). The flow is based on experimental results for 16:4 mmol/s He: $\text{O}_2$  through a 400 W RF discharge, modeling a titration flow of 0.2 mmol/s of  $\text{NO}_2$ . The pressure is 12.6 Torr.

### 3.4 Trace argon actinometry

Another technique pursued by our group is argon actinometry, applying theory as described by Pagnon<sup>17</sup>, and making measurements of the actinometer ratio in the afterglow of RF discharge using a similar setup to that suggested by Braginskiy<sup>18</sup>. In this technique, a small amount of argon is combined with the primary discharge effluent, which flows through a secondary low-power discharge. Spectra are taken within the discharge to measure the ratio of atomic oxygen emissions to argon emissions. The intensity of the emissions can be expressed in the fashion

$$I_{\text{O}^*} = C_{\text{det}} \left\{ \frac{h\nu_{ij} A_{ij} k_e^{\text{O}^*} n_e}{\Sigma A_{ij} + k_Q[\text{Q}]} \right\}_{\text{O}^*} [\text{O}] \quad (8)$$

$$I_{\text{Ar}^*} = C_{\text{det}} \left\{ \frac{h\nu_{ij} A_{ij} k_e^{\text{Ar}^*} n_e}{\Sigma A_{ij} + k_Q[\text{Q}]} \right\}_{\text{Ar}^*} [\text{Ar}] \quad (9)$$

where  $n_e$  is the electron density,  $h\nu_{ij}$  is the photon energy emitted by the excited state,  $A_{ij}$  is the Einstein coefficient of the observed transition, and  $\Sigma A_{ij}$  is the sum of the radiative de-excitation processes from the upper state of the transition. The rates  $k_e$  and  $k_Q$  respectively are the excitation rate of the upper state (from the ground state) and the quenching rate of the upper state by quencher density  $[\text{Q}]$ .  $C_{\text{det}}$  is a constant associated with the detection system, which we assume to be constant for all emission lines, considering that the observation volume is unchanged. The ratio of equations (8) and (9) can be taken to get a simple proportion

$$\frac{I_{\text{O}^*}}{I_{\text{Ar}^*}} = C_{\text{O/Ar}} \frac{[\text{O}]}{[\text{Ar}]} \quad (10)$$

where  $C_{\text{O/Ar}}$  is the ratio of the bracketed terms in (8) and (9). Thus the level of atomic oxygen can be determined by measuring the ratio of oxygen and argon lines, and multiplying by  $[\text{Ar}]/C_{\text{O/Ar}}$  to get  $[\text{O}]$ . Alternatively, one can use the atomic flow rates from the  $\text{NO}_2$  titration to calibrate the intensity ratio to the atom density, using the relation

$$\frac{I_{O^*} [Ar]}{I_{Ar^*} [O_2]} = C_{O/Ar} \frac{[O] [Ar]}{[Ar] [O_2]} = F_{cal} \left( \frac{[O]}{[O_2]} \right)_{NO_2\text{-titr.}} \quad (11)$$

where  $F_{cal}$  is an experimentally determined calibration factor, and  $([O]/[O_2])_{NO_2\text{-titr.}}$  is the atomic density ratio obtained from the  $NO_2$  titration method.

Preliminary actinometry experiments were recently performed under typical fast flow laser operating conditions, making a direct comparison between the actinometry and  $NO_2$  titration techniques. The comparison made use of a secondary discharge, a CCD camera for the actinometry ( $O^*$  and  $Ar^*$  signals), and a PMT downstream of a tangential injector for the  $NO_2$  titration. The  $NO_2$  injector was situated 18 cm downstream of the primary longitudinal hollow-cathode RF discharge, with the PMT fiber-coupled to a diagnostic block 49.5 cm downstream of the injection point. The secondary discharge was capacitively-coupled RF, using 2.5 cm wide copper electrodes separated by 11 cm. This second discharge was located about 35 cm downstream of the primary electrode region, in between the  $NO_2$  injector and the PMT. The fiber-coupling for the spectrometer and CCD was placed  $\sim 2.5$  cm from the glass tube surface directly between the secondary electrodes. Using this dual-diagnostic setup, titrations were first performed sweeping primary RF system power in the range of 100 to 800 W, and determining  $[O]$  using the  $NO_2$  titration procedure. Then, a 20-W secondary discharge was engaged, and the primary power sweep was repeated while capturing the intensities of the  $O^*(777\text{-nm})$  and  $Ar^*(750.4\text{-nm})$  lines with the spectrometer and CCD. During this portion of the experiment, scans were taken both with and without the secondary discharge to determine the significance of the  $O^*(777\text{-nm})$  produced by the primary discharge in the secondary discharge region. A few scans were also taken with only the secondary discharge engaged, to gauge the amount of atoms produced by the secondary. The flows used in the experiment were 16:3:0.05 mmol/s He: $O_2$ :Ar at  $\sim 6.5$  Torr. The mixture and pressure were chosen due to the expectation of significant yields of oxygen atoms based on previous experiments.

Figure 11 shows a comparison between the oxygen atom flow rates determined from the  $NO_2$  titration technique and the calibrated argon actinometry technique resulting from the experiment described above. The flow rate determined from the actinometry is the ratio of the  $O^*(777\text{-nm})$  and  $Ar^*(750.4\text{-nm})$  lines times the input ratio of Ar to  $O_2$  multiplied by a calibration constant,  $1/F_{cal}$ , as in Eqn. (11), with the small baseline signal due to the 20-W secondary subtracted. The calibration constant was found by minimizing the square-root sum of the squares of the difference between the calibrated actinometry data and the linear fit to the titration data. The agreement of the two data sets is encouraging. However, the influence of each discharge on the other must be considered and minimized. The 20-W secondary discharge produces a small amount of dissociation by itself, corresponding to  $\sim 0.065$  mmol/s on the calibrated scale (removed in Fig. 11). Also, the primary discharge pumps the  $O^*$  in the secondary discharge region through UV excitation. Figure 12 shows the  $O^*(777\text{-nm})$  signal with and without the secondary discharge. The  $O^*$  signal in the secondary region with only the primary discharge excitation is at most 3% of the signal with the secondary engaged and can easily be compensated for during calibration.

In another actinometry experiment, the effect of NO on the technique was investigated, looking at the  $O^*(777\text{-nm})$  and  $Ar^*(750.4\text{-nm})$  emissions within the primary longitudinal RF discharge. Again using the spectrometer and CCD to measure intensities, the ratio of the oxygen line to argon lines was taken as a function of power for a discharge flow of 16:3:0.05 He: $O_2$ :Ar at 12.5 Torr. This result, shown in Fig. 13 is encouraging, considering that the actinometry technique measures a linear response of atoms with power in the presence of NO, however, the effects of NO on the discharge pumping of argon and oxygen states illustrates a higher level of complexity. In the data given in Fig. 13, the addition of NO resulted in a reduction of all three emissions, which indicates that the pumping mechanisms are affected. A collision between argon metastables and NO most likely results in the ionization of NO, removing the former from the excitation routes for  $Ar^*$  and  $O^*$ .

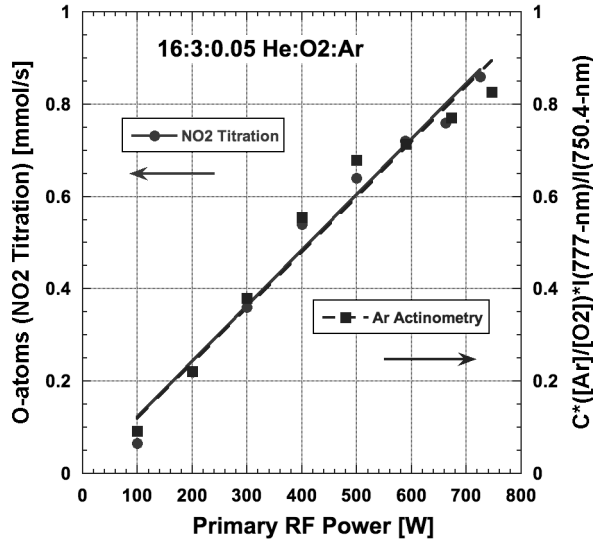


Figure 11. A comparison of the Ar actinometry and NO<sub>2</sub> titration techniques for determining O-atoms. The mixture used is 16:3:0.05 He:O<sub>2</sub>:Ar at ~ 6.5 Torr. The secondary discharge was 20-W capacitive RF. The calibration constant C=1.04.

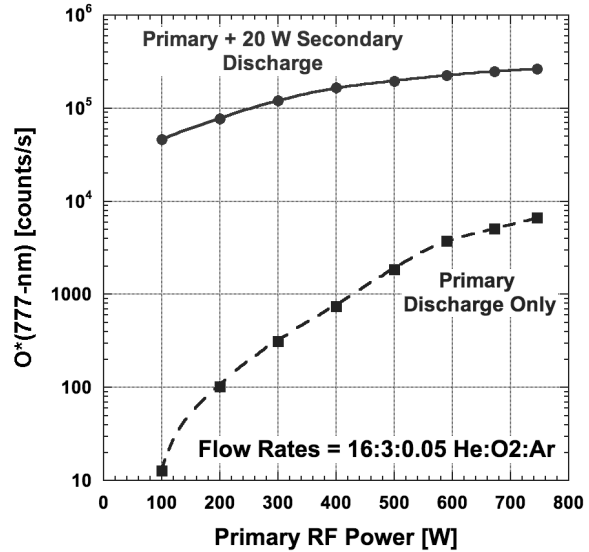


Figure 12. The influence of the primary discharge on O\*(777-nm) signal in the secondary discharge region. The mixture used is 16:3:0.05 He:O<sub>2</sub>:Ar at ~ 6.5 Torr. The secondary discharge was a 20-W capacitive RF.

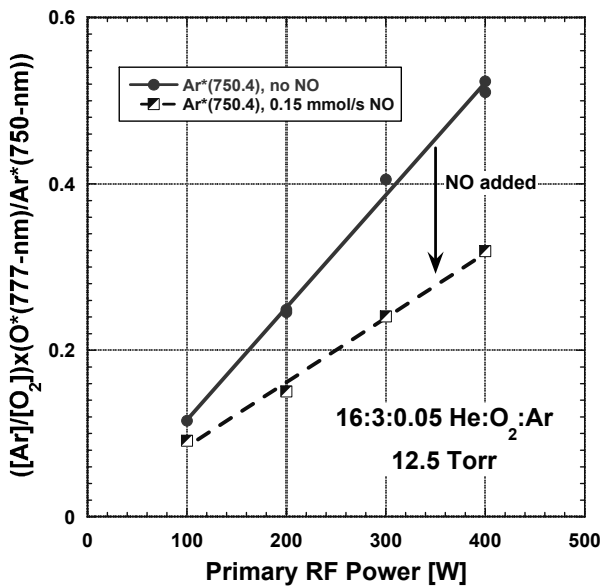


Figure 13. Argon actinometry ratio in the primary longitudinal discharge with and without NO. The discharge flow is 16:3:0.05 He:O<sub>2</sub>:NO at 12.5 Torr. The measurement is proportional to atomic oxygen, but calibration factors have not been established for cases with NO.

#### 4. THE SPATIAL BEHAVIOR OF SINGLET OXYGEN

Previous works<sup>5</sup> have reported on the decay of singlet oxygen in the post discharge region of the ElectricOIL system. The typical observed effect was that O<sub>2</sub>(a) is relatively invariant with flow distance, while O<sub>2</sub>(b) decays rapidly in the post discharge region due to quenching by atoms. This behavior is consistent over a variety of flow conditions, but the spatial behavior of each is strongly affected by the presence of NO<sub>x</sub> and the lasing species I\*, and the influence of these on atom concentrations<sup>12</sup>.

#### 4.1 Spatial behavior of O<sub>2</sub>(a) and O<sub>2</sub>(b) produced in He:O<sub>2</sub> discharge

In recent ElectricOIL experiments, higher flow rates of oxygen have been examined in an attempt to scale to increased laser powers. This effort has led to a host of problems associated with relative oxygen atom flow rates, decreased yield at higher flow rates (lower specific power), required iodine flow rates, and flow temperature control. The primary problem is that as oxygen flow is increased, the amount of power deposited per molecule of oxygen decreases for a given power supply. Thus, in a confined system, getting more power flux stored in O<sub>2</sub>(a) may be possible, but this is at the expense of lowering yields. In addition, the level of dissociation changes (see Figs. 2 and 3) affecting the dynamics of the system when iodine is present.

Figures 14 and 15 show the spatial behavior of O<sub>2</sub>(a) and O<sub>2</sub>(b) respectively for various RF power settings downstream of the longitudinal hollow-cathode discharge. The flows for the case shown are 33:10:0.15 mmol/s He:O<sub>2</sub>:NO. As in previous work<sup>5</sup>, the O<sub>2</sub>(a) yield is relatively invariant with distance for these fast flow conditions. Also, the decay of O<sub>2</sub>(b) is fairly rapid due to quenching by atomic oxygen, even in the presence of NO which reduces oxygen atoms<sup>4</sup>. The yields shown here are based on a constant proportion calibration between intensity integral and density, which is derived using a calibrated surface source from Keo Consultants. In the most extreme case, 600 W RF, the temperature near the discharge exit is about 500 K (as determined from the O<sub>2</sub>(b) rotational spectra) decreasing to ~400 K over 65 cm. This produces conditions favorable for positive gain with expansion through a supersonic nozzle reducing the temperature by a factor of approximately 2, and O<sub>2</sub>(a) yield near 12%.

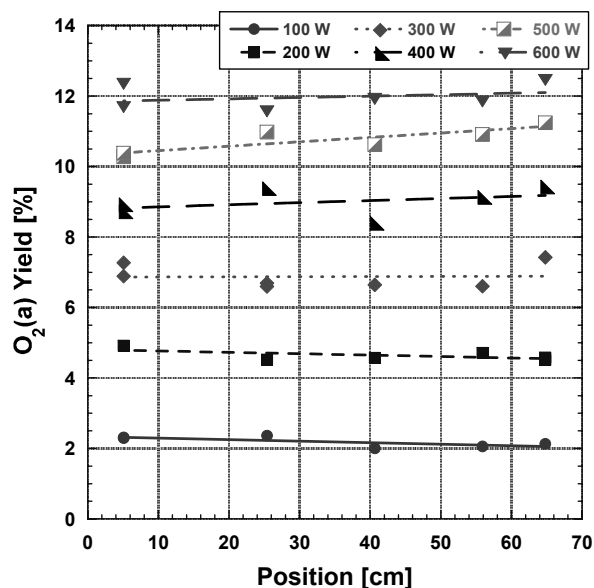


Figure 14. O<sub>2</sub>(a) yield as a function of distance for 33:10:0.15 mmol/s He:O<sub>2</sub>:NO at 16 Torr. The position is referenced to the trailing edge of the downstream grounded electrode.

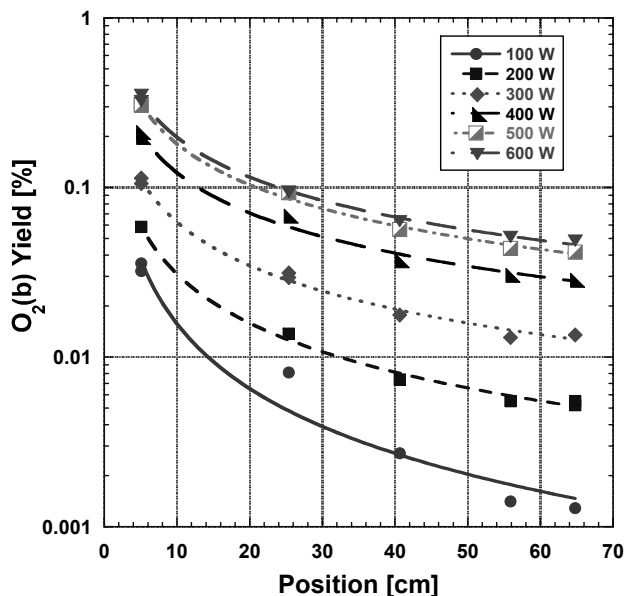


Figure 15. O<sub>2</sub>(b) yield as a function of distance for 33:10:0.15 mmol/s He:O<sub>2</sub>:NO at 16 Torr. The position is referenced to the trailing edge of the downstream grounded electrode.

#### 4.2 Enhanced O<sub>2</sub>(a) production with NO<sub>x</sub>

Figure 16 shows the effect of NO and NO<sub>2</sub> added in three conditions for a discharge flow of 16:3 He:O<sub>2</sub>. The three conditions are (i) NO<sub>2</sub> downstream of the discharge, (ii) NO downstream of the discharge, and (iii) NO through the discharge. In the setup for this experiment, the downstream injector is 15.24 cm downstream of the downstream hollow cathode, and the measurement is made 65.4 cm from the injection point. For these flow distances, the injection of either NO or NO<sub>2</sub> downstream leads to approximately the same benefit for O<sub>2</sub>(a) yield (~9 to 13.5%, a significant 50% increase in magnitude), invariant after ~0.03 mmol/s NO<sub>x</sub>. This beneficial effect is likely due to branching into O<sub>2</sub>(a) as oxygen

atoms are recombined by reaction (2) combined with recycling of  $\text{NO}_2$  by reaction (3). With similar amounts of  $\text{NO}$  added through the discharge instead, the yield is increased to about 16% (a dramatic magnitude increase of approximately 80%). The cause for this additional boost in  $\text{O}_2(\text{a})$  is a subject of considerable speculation, and is likely a combination of  $\text{O}_2(\text{a})$  resulting from reaction (3), and the effects of  $\text{NO}$  on discharge dynamics. Figure 17 shows a similar  $\text{NO}$  injection case, plotting the filtered PMT air-glow signal and 1268 nm  $\text{O}_2(\text{a})$  emission as a function of distance for 16:3 mmol/s  $\text{He}:\text{O}_2$  at 19.9 Torr, with 500 W RF. In both cases (upstream and downstream injection), the air afterglow, which is proportional to oxygen atom density, decays to zero while  $\text{O}_2(\text{a})$  density increases. When  $\text{NO}$  is flowed through the discharge, the air afterglow is reduced to about a third of that when  $\text{NO}$  is injected downstream. Assuming that the local  $\text{NO}$  density is the same in either case, this suggests a proportional decrease in oxygen atom flow rate, similar to the reduction in extinguishing point seen in Fig. 8 for other operating conditions. The increase in  $\text{O}_2(\text{a})$  density over the flow distance is similar for both injection points, with the  $\text{NO}$  through the discharge resulting in significantly higher yields. The data with  $\text{NO}_x$  injection downstream indicate that the effect is dual natured, with components due to both discharge effects and atom recombination. However, the flow distance added (distance between primary electrode and normal downstream injection point) when the  $\text{NO}$  is run through the discharge is significant (40-65 cm depending on case), which is consistent with increases due to recombination alone.

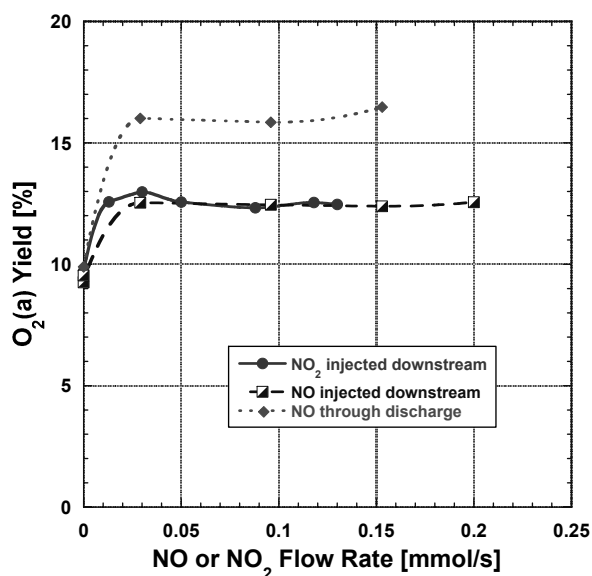


Figure 16. The effect of  $\text{NO}_x$  injection on the behavior of  $\text{O}_2(\text{a})$  in 16:3 mmol/s  $\text{He}:\text{O}_2$ , at 500 W RF, 12.5 Torr.

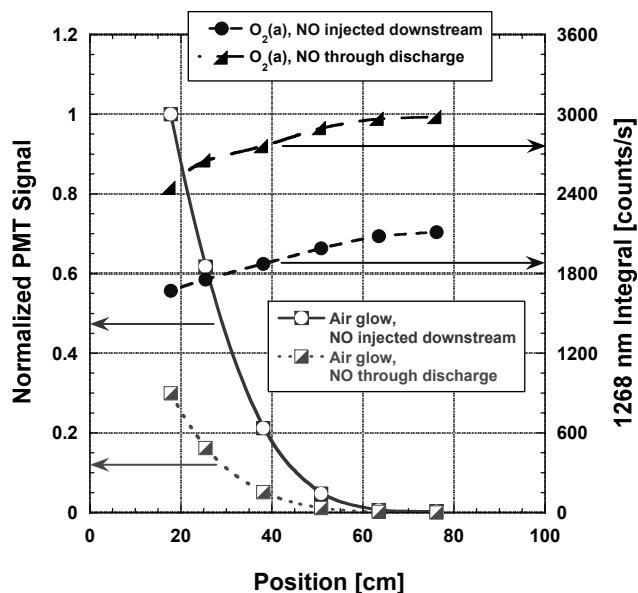


Figure 17. Spatial behavior of PMT signal and  $\text{O}_2(\text{a})$  density in 16:3 mmol/s  $\text{He}:\text{O}_2$ , at 500 W RF, 19.9 Torr. The  $\text{NO}$  flow is 0.2 mmol/s. Position is referenced to the downstream injector, which is 42 cm downstream of driven electrode. The atom flow rate in the downstream injection case was 0.32 mmol/s (determined from  $\text{NO}_2$  titration).

## 5. SUMMARY

This work has outlined the diagnostic techniques being applied in our laboratory to detect trends in atomic oxygen, and study the interplay of  $\text{NO}_x$  in the hybrid ElectricOIL system. Investigations have included the use of two air afterglow methods, and a trace argon actinometry technique which produce results that are in reasonable agreement. Application of air afterglow techniques was found to be difficult when  $\text{NO}$  was used as a sensitizer to benefit  $\text{O}_2(\text{a})$  production, due to the glow intensity behaviors for the flow rates of interest. This result prompted application of the argon actinometry technique, which shows good agreement with afterglow methods, and produced consistent results in the presence of  $\text{NO}$ . For scaled up diluted oxygen flow rates in the presence of  $\text{NO}$ , the spatial behavior of singlet oxygen was found to be consistent with previous data (without  $\text{NO}$  in the flow), resulting in  $\text{O}_2(\text{a})$  yields invariant with distance, and small yields of  $\text{O}_2(\text{b})$  with fairly rapid decay despite the loss of atoms by recombination with  $\text{NO}_x$ . Studies of  $\text{NO}_x$  injection both

within and downstream of the discharge have indicated that the benefits to  $O_2(a)$  seen in previous work are due primarily to atom recombination by NO followed by a significant branching to  $O_2(a)$  produced by the  $O+NO_2$  reaction and not lowering of ionization potential as originally reported.

## ACKNOWLEDGEMENTS

This work was supported by the Air Force Office of Scientific Research (AFOSR), and by CU Aerospace internal research and development funds. The authors would like to gratefully acknowledge the invaluable discussions and support of: T. Madden (Air Force Research Laboratory); G. Hager (Univ. of New Mexico); M. Kushner (Iowa State University); K. Morokuma (Emory University); G. Perram (Air Force Institute of Technology); M. Berman (AFOSR); L. Piper. We would also like to thank B. Wheaton and A. Roberts for their technical assistance.

## REFERENCES

1. W. McDermott, N. Pchelkin, D. Benard, and R. Bousek, *Appl. Phys. Lett.* **32** (8) 469 (1978).
2. Zaleskii, V. Yu., *Zh. Eksp. Teor. Fiz.*, **67** 30 (1974) [*Sov. Phys. JETP* **40** (1) 14 (1975)].
3. G. Fournier, J. Bonnet, and D. Pigache, *J. Physique* **41** Colloque C9, 449 (1980).
4. D.L. Carroll, J.T. Verdeyen, D.M. King, B.S. Woodard, L.W. Skorski, J.W. Zimmerman, and W.C. Solomon, *IEEE J. Quant. Elect.* **39** (9) 1150 (2003).
5. D.L. Carroll, J.T. Verdeyen, D.M. King, B.S. Woodard, J.W. Zimmerman, L.W. Skorski, and W.C. Solomon, "Recent Experimental Measurements of the ElectricOIL System," AIAA Paper 2003-4029 (2003).
6. J. Schmiedberger, S. Hirahara, Y. Ichinoche, M. Suzuki, W. Masuda, Y. Kihara, E. Yoshitani, and H. Fujii, *SPIE* Vol. **4184** 32 (2001).
7. A.E. Hill, in *Proc. of the International Conf. on Lasers 2000*, ed. by V. Corcoran and T. Corcoran (STS Press, McClean, VA, 2001) 249.
8. A.A. Ionin, Y.M. Klimachev, A.A. Kotkov, I.V. Kochetov, A.P. Napartovich, L.V. Seleznev, D.V. Sinitsyn, and G.D. Hager, *J. Phys. D: Appl. Phys.* **36** 982 (2003).
9. T.V. Rakhimova, A.S. Kovalev, A.T. Rakhimov, K.S. Klopovsky, D.V. Lopaev, Y.A. Mankelevich, O.V. Proshina, O.V. Braginsky, and A.N. Vasilieva, "Radio-Frequency Plasma Generation of Singlet ( $a^1\Delta_g$ ) Oxygen in  $O_2$  and  $O_2:Ar$  (He) Mixtures," AIAA Paper 2003-4306 (2003).
10. Carroll, D. L. et. al. *Appl. Phys. Lett.*, 2004
11. Carroll, D. L. et. al. *Appl. Phys. Lett.*, 2005
12. D. L. Carroll, J. T. Verdeyen, D. M. King, J. W. Zimmerman, J. K. Laystrom, B. S. Woodard, G. F. Benavides, K. Kittell, and W. C. Solomon, "Path to the measurement of positive gain on the 1315 nm transition of atomic iodine pumped by  $O_2(a^1\Delta)$  produced in an electric discharge," *IEEE J. Quant. Elect.*, vol. 41, no. 2, pp. 213–223, 2005.
13. A. D. Palla, D. L. Carroll, J. T. Verdeyen, and W. C. Solomon. "Mixing Effects in Post-Discharge Modeling of ElectricOIL Experiments." to be published in *J. Appl. Phys.* (2006)
14. Kaufman, F. (1958). *Proc. Roy. Soc. A*, **247**, 123.
15. D.S. Stafford and M.J. Kushner, *J. of Appl. Phys.* **96** (5) 2451 (2004).
16. L. G. Piper, G. E. Caledonia, and J. P. Kennealy, *J. Chem. Phys.* **75**, 2847 (1981).
17. Pagnon, D., Amorim, J., Nahorny, J., Touzeau, M., Vialle, M., (1995). "On the use of actinometry to measure the dissociation in  $O_2$  DC glow discharges: determination of the wall recombination probability," *J. Phys. D: Appl. Phys.* **28**, 1856-1868.
18. Braginskiy, O., Vasilieva, A., Klopovskiy, K., Kovalev, A., Lopaev, D., Proshina, O., Rakhimova, T., Rakhimov, A., "Singlet oxygen generation in  $O_2$  flow excited by RF discharge: I. Homogeneous discharge mode:  $\alpha$ -mode." *J. Phys. D: Appl. Phys.* **38**, 3609-3625 (2005).
19. R. Atkinson, D. L. Baulch, R. A. Cox, R. F. Hampson Jr., J. A. Kerr, M. J. Rossi, and J. Troe, *J. of Phys and Chem. Ref. Data*, vol. 26, no. 3, pp. 550–962, 1997.